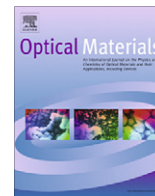




Contents lists available at ScienceDirect

Optical Materials

journal homepage: www.elsevier.com/locate/optmat

Mechanism of the liquid-phase sintering for Nd:YAG ceramics

R. Boulesteix^a, A. Maître^{a,*}, J.-F. Baumard^a, C. Sallé^b, Y. Rabinovitch^b^a Laboratoire Science des Procédés Céramiques et de Traitements de Surface, UMR CNRS 6638, UFR Sciences et Techniques, 123 Avenue Albert-Thomas, F-87060 LIMOGES Cedex, France^b CILAS, Bâtiment ESTER, BP 76923, F-87069 LIMOGES Cedex, France

ARTICLE INFO

Available online xxxx

Keywords:

Nd:YAG
Sintering mechanism
Modeling
Liquid phase
Silica

ABSTRACT

The mechanisms of the solid-state sintering of pure Nd:YAG and of the liquid-phase sintering of silica-doped Nd:YAG ceramics have been studied during the present work.

On one hand, the densification mechanism of undoped Nd:YAG ceramics which obeys to a solid-state sintering has been investigated. It appeared from the kinetical tests performed under isothermal conditions (between 1723 and 1823 K) that densification is a thermally activated process during the intermediate stage of solid-state sintering. The activation energy so-determined (600 kJ mol^{-1}) was attributed to densification controlled by the grain boundary diffusion of rare-earth elements.

On the other hand, the kinetical analysis of the liquid-phase sintering of silica-doped Nd:YAG materials has been carried out for temperature ranging between 1723 and 1823 K, *i.e.*, for any temperature higher than the melting point (1660 K) of the silica-rich secondary phase which adopts the eutectic composition in $\text{SiO}_2\text{-Al}_2\text{O}_3\text{-Y}_2\text{O}_3$ system. Densification rate increases versus increasing liquid content and sintering temperature. The activation energies ranged from 1145 to 986 kJ mol^{-1} over the relative density range of 70% to 90%, respectively. The high activation energies have been correlated to the solution-precipitation stage of sintering for which the interface reaction would be the rate-controlling step.

© 2008 Elsevier B.V. All rights reserved.

1. Introduction

YAG (Yttrium Aluminum Garnet– $\text{Y}_3\text{Al}_5\text{O}_{12}$) belongs to the family of the attractive materials to which attention is paid in view of applications in the field of high energy lasers. Appropriate rare earth dopants (mainly Nd^{3+}) are added in small proportions to the matrix due to their luminescent properties. They enter into solid solution within the garnet crystallographic lattice where they substitute Y^{3+} ions species owing to size and electric charge criteria.

Low duration and low cost of manufacturing, absence of severe limitation in size and geometry make the Nd:YAG ceramics attractive with comparison to single crystals [1–3]. Ikesue et al. [4] were the first to demonstrate the possibility of elaborating transparent Nd:YAG ceramics with the required optical properties. In term of laser application, recent works [5,6] have shown that transparent polycrystalline Nd:YAG ceramics are equivalent or even better than single crystals grown by the Czochralski method. Nevertheless, the ceramic route which rests on the sintering of mixtures of reactive oxides (Al_2O_3 , Y_2O_3 and Nd_2O_3) requires the control of each step during the elaboration process.

The reaction sequence of the “pure” Nd:YAG sintering (*i.e.* without silica) from $\text{Al}_2\text{O}_3/\text{Y}_2\text{O}_3/\text{Nd}_2\text{O}_3$ mixtures prepared to the stoi-

chiometric proportions has been reported in literature [2,7,8]. Three successive reactions occur between 1173 and 1673 K. The first corresponds to the $\text{Y}_4\text{Al}_2\text{O}_9$ phase formation. The second transformation leads to the YAP formation (YAIO_3 -perovskite structure) and finally residual Al_2O_3 reacts with the YAP phase to form YAG. For upper temperatures, shrinkage is observed due to the densification of YAG [7]. From literature, it is well known that the use of sintering aids (*e.g.* MgO or SiO_2) [9,10] is necessary to reach fully dense and transparent Nd:YAG ceramics. Recently, Sallé et al. [7] pointed out that small additions of silica enhance densification kinetics and inhibit the abnormal grain growth at the final stage of sintering. The formation of the liquid phase which appears at around 1660 K would result from the solid–solid reaction between silica and YAG particles. The chemical composition of the liquid phase so-formed was reported to belong to the eutectic compound in $\text{SiO}_2\text{-Al}_2\text{O}_3\text{-Y}_2\text{O}_3$ pseudo-ternary diagram [11–13]. Previous studies [14–16] have already reported the same beneficial role of silica additions upon sintering by suggesting the increase of grain boundary (GB) diffusion coefficient or the decrease of GB surface energy in presence of secondary phases. Based on structural considerations, Kuklja [17] proposed that the silica effect is also correlated to a solid solution formation by substitution of Al^{3+} by Si^{4+} in tetrahedral sites. This transformation leads to the formation of Y^{3+} vacancies which would enhance the lattice diffusion coefficient, and consequently, improve the YAG densification kinetics.

* Corresponding author. Tel.: +33 5 55 45 74 63; fax: +33 5 55 45 75 86.
E-mail address: alexandre.maitre@unilim.fr (A. Maître).

Under the hypothesis of a liquid-phase sintering mechanism for silica-doped Nd:YAG ceramics, the effectiveness of a liquid phase during sintering cannot be properly identified unless the rate-controlling mechanism responsible for densification is known. Consequently, the purpose of the present study is firstly to undertake the kinetic analysis under isothermal conditions of the intermediate-stage of the densification during the liquid-phase or the solid-state sintering of Nd:YAG ceramics (*i.e.* with or without silica additions, respectively). Such quantitative information, correlated to microstructural evolution during sintering, will yield insight into the role of silica in the improvement of densification kinetics of Nd:YAG ceramics.

2. Experimental

2.1. Powder preparation for sintering

The manufacturing process used during this work is similar to that reported by Rabinovitch et al. [18].

To prepare the powders for pressing, submicron alpha alumina (Baikowski, purity > 99.99%), yttria (Alfa Aesar, purity > 99.99%) and neodymium oxide (Alfa Aesar, purity > 99.99%) were mixed to reach the composition $Y_{2.94}Nd_{0.06}Al_5O_{12}$ after thermal treatment. For silica-doped samples, nanosized silica particles (Alfa Aesar, purity > 99.8%), used as sintering aid, were added in contents ranging from 0 wt.% to 0.3 wt.%. After ball milling in a solvent (water + binder), the powder was uniaxially pressed at 200 MPa in a steel die to make pellets nominally 17 mm in diameter by 5 mm high. Prior to sintering, the organics were completely removed by heating the samples in air.

2.2. Sintering

Sintering was conducted under isothermal conditions and vacuum ($P_T \leq 10^{-2}$ Pa) between 1723 and 1923 K with various soaking times and cooled down to room temperature. The specimens were placed in an alumina crucible. A heating rate of 15 K min⁻¹ (*i.e.* in the upper range accessible with the present tungsten mesh-heated furnace) was used. Therefore, these sintering temperatures were chosen to yield equilibrium liquid phases with Nd:YAG when silica was introduced [7].

In parallel, further dilatometric experiments were carried out to establish the kinetics of densification for Nd:YAG with or without silica. So, the shrinkage was followed as a function of time and temperature by dilatometry (Thermal Mechanical Analyzer, TMA 92, Setaram[®], France). These thermal treatments were achieved under vacuum with a heating rate of 20 K min⁻¹ up to temperatures ranging between 1723 and 1823 K.

2.3. Density measurement and microstructural observations

Relative densities of Nd:YAG samples after sintering were measured by using either geometrical or the Archimedes method. The theoretical density of fully dense YAG was taken as 4.55 g cm⁻³.

After cooling, the sintered samples were polished and thermally etched under air at 100 K below the sintering temperature to investigate the microstructure by Scanning Electron Microscopy (SEM, Philips[™] XL30 and FEG-SEM, JEOL[™] 7400). The mean grain size of etched samples was determined, thanks to image analysis software (Scion software, Scion Corp., USA). The equivalent disc diameter was chosen as a parameter for size evaluation. For each sample, average grain size measurements done over 300 grains (*i.e.* from at least 5 images) lead to an error of about 2.5%.

3. Results and discussion

3.1. Sintering map of Nd:YAG ceramics

The experimental data (grain size, relative density) issued from the sintering attempts which were performed between 1723 and 1923 K have been reported in the corresponding sintering map (Fig. 1). The observation of the grain size (G) versus relative density (ρ) trajectories for undoped and silica-doped Nd:YAG specimens allow to establish correlation between densification and microstructure evolution and to discuss the influence of silica on microstructure development.

From Fig. 1, it is interesting to notice that three types of microstructures are obtained depending on the experimental parameters (whatever the silica content): porous materials (open porosity, relative density between 60% and 90%) with submicrometer grain size (around 500 nm), dense ceramics (closed porosity, relative density (ρ) between 90% and 97%) with a micrometer grain size (around 2 μ m) and fully dense material with an average grain size larger than 3 μ m. It is well known that the grain size-density trajectory is a function of the relative ratio of the densification rate to the grain growth rate. So, at the final stage of densification ($\rho > 97\%$), the flattening of the G - ρ trajectories that is observed in the silica-doped Nd:YAG materials reflect the fact that the doping enhances the densification rate relative to the grain-growth rate. At 1973 K, the average grain size of silica-doped material remains around 5 μ m while it increases up to 11 μ m for pure Nd:YAG. Consequently, silica seems to inhibit exaggerated grain growth and leads to a suitable homogeneous microstructure to obtain transparent ceramics.

In the next part, the densification mechanisms during the intermediate stage of solid-state and liquid-phase sintering of Nd:YAG ceramics (*i.e.* for relative density ranging between 70% and 95%) have been investigated.

3.2. Sintering mechanisms

3.2.1. Solid-state sintering of Nd:YAG ceramics

Fig. 2 depicts the relative density as a function of sintering time at temperatures ranging between 1723 and 1823 K for “pure” Nd:YAG samples. These data have been obtained from shrinkage measurements thanks to the dilatometry device. The shrinkage is considered isotropic during the present work. Then the relative density is calculated from the following expression:

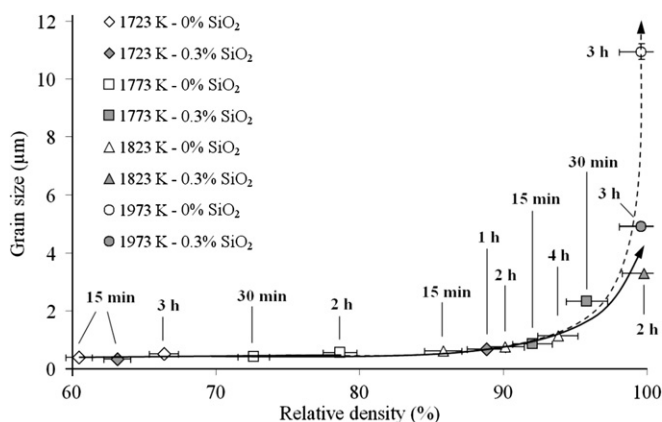


Fig. 1. Sintering map of Nd:YAG ceramics containing 0.3 wt.% SiO₂ (closed symbols) or silica free (open symbols). Sintering temperature and dwelling time ranging, respectively, from 1723 K to 1973 K and 15 min to 4 h. Sintering trajectories for samples with or without silica were reported as full and dotted lines, respectively.

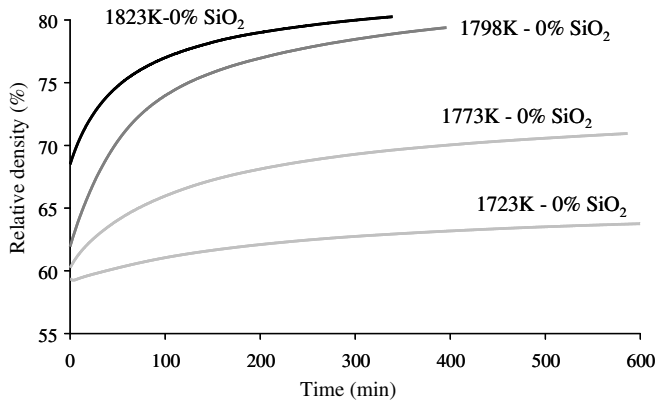


Fig. 2. Densification curves of undoped Nd:YAG samples as a function of sintering time at different soaking temperatures. Heating rate was 15 K min^{-1} .

$$\rho = \frac{\rho_0}{\left[1 - \left(\frac{\Delta L}{L_0}\right)\right]^3} \quad (1)$$

where ρ denotes the relative density at instant t , ρ_0 the initial relative density, ΔL the shrinkage at the same soaking time t , and L_0 the initial length of the specimen. Under these conditions, the relative density increases from 60% to 80%, an interval which corresponds to the intermediate stage of densification of the Nd:YAG samples. From Fig. 2, it is observed that the densification process is thermally activated: the higher the sintering temperature, the faster the densification occurs during sintering.

The densification data reported in Fig. 2 were analyzed according to a conventional sintering mechanism governed by either lattice diffusion or grain-boundary diffusion. The rate equation for these mechanisms is usually written as [19,20]:

$$\frac{1}{\rho} \frac{d\rho}{dt} = \frac{f(\rho)}{kTG^m} D_0 \exp\left(-\frac{E_a}{RT}\right) \quad (2)$$

where ρ is the relative density, t is time, T is the absolute temperature, $f(\rho)$ is function only of the relative density, G is the mean grain size, D_0 is the pre-exponential coefficient of diffusion, R is the gas constant and E_a is the apparent activation energy. For volume diffusion, $D_0 = (D_v)_0$ and $m = 3$; for grain boundary diffusion, $D_0 = (\delta D_b)_0$ where δ is the grain boundary thickness and $m = 4$.

With the case of a polynomial fit of the data files representing the evolution of the relative density versus firing time at different soaking temperatures, it is possible to have access to the variation of the densification rate $\left(\frac{1}{\rho} \times \left(\frac{d\rho}{dt}\right)\right)$ as a function of sintering time.

Then $\left(TG^m \frac{1}{\rho} \left(\frac{d\rho}{dt}\right)\right)$ function is plotted versus reciprocal temperature ($1/T$) at a given relative density (ρ) using the particle-size data determined for the same samples. This procedure has been followed for two relative densities (70% and 80%). As shown in Fig. 3, a straight line fit of all the data can be obtained by assuming $m = 4$ whatever the relative density value. The activation energy implied by this plot is $595 \pm 70 \text{ kJ mol}^{-1}$ which may be identified to the activation energy of grain boundary diffusion. Therefore, this latter value should be consistent with the activation energy for the grain-boundary diffusion of the rare-earth element (i.e. Y^{3+} : $E_a = 565 \pm 85 \text{ kJ mol}^{-1}$ [21] and Nd^{3+} : $E_a = 637 \pm 90 \text{ kJ mol}^{-1}$ [22]) in Nd:YAG specimens. It is worth to notice that these grain boundary diffusion coefficients were determined (in Ref. [21] and [22]) thanks to rare-earth concentration profiles determined by Secondary Ion Mass Spectrometry (SIMS) techniques from annealing between 1673 and 1873 K of rare-earth oxides thin films deposited on YAG substrates. From sintering and diffusion experiment results, it is then concluded that densification during the intermedi-

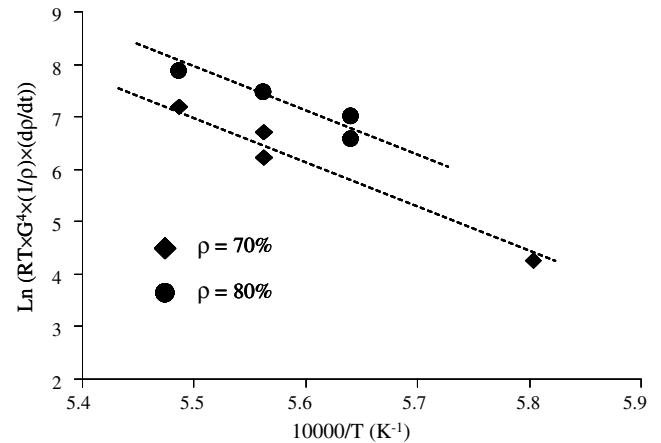


Fig. 3. Size-compensated densification rate versus reciprocal temperature with $m = 4$ for undoped Nd:YAG specimens at various relative densities (70% and 80%).

ate stage of solid-state sintering of the undoped Nd:YAG specimens is controlled by the rare-earth grain boundary diffusion.

3.2.2. Effect of silica on densification mechanism

The densification kinetics has been followed as a function of the two process variables: silica content and temperature.

Data presenting the dependence of densification rate on the starting silica content from 0 wt.% to 0.3 wt.% at 1773 K are shown in Fig. 4. Clearly, the densification rate increases significantly with increasing liquid volume content: indeed, for a given relative density, the densification rate obtained with 0.3 wt.% SiO_2 increases by two orders of magnitude with respect to those observed without any silica addition (see Table 1). These results confirm the effectiveness of the silica addition for liquid-phase sintering of Nd:YAG samples.

Fig. 5 depicts the densification kinetics of Nd:YAG ceramics containing 0.3 wt.% SiO_2 during firing at 1723, 1773, 1798 and 1823 K. These curves demonstrate that the liquid-phase Nd:YAG sintering

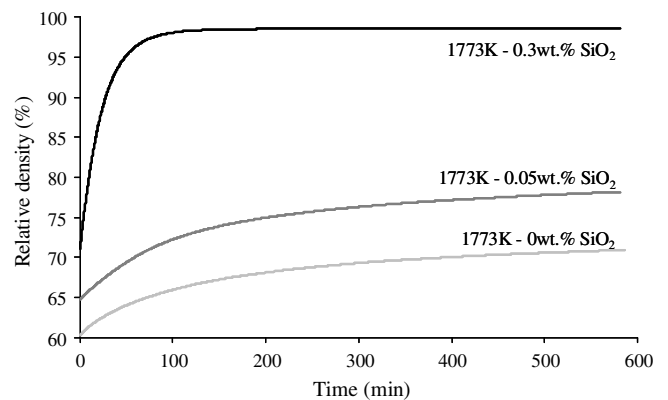


Fig. 4. Densification curves of silica-doped Nd:YAG samples as a function of sintering time at different soaking temperatures. Heating rate was 15 K min^{-1} .

Table 1

Densification rates $\left(\frac{1}{\rho} \times \left(\frac{d\rho}{dt}\right)\right)$ for different silica-doped Nd:YAG samples at 1773 K and for a given relative density (75%)

Silica content (wt.%)	Densification rate (10^{-6} s^{-1})
0	3.6
0.05	14
0.3	330

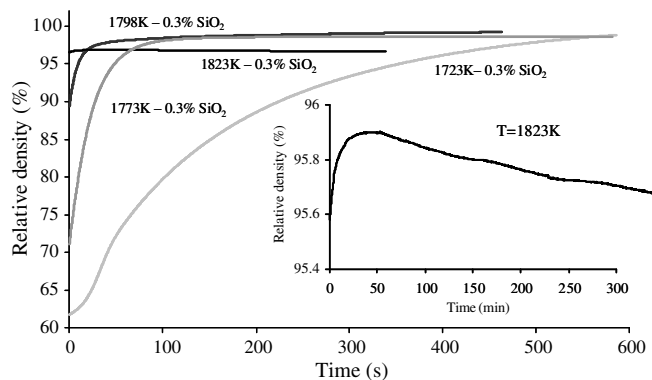


Fig. 5. Densification curves of Nd:YAG doped with 0.3 wt.% SiO₂ as a function of time at different sintering temperatures with a heating rate of 15 K min⁻¹.

is thermally activated. However, at higher firing temperature (*i.e.* 1823 K), the relative density maximum is followed by slight dedensification at longer sintering times. The dedensification effect could be explained from different hypotheses:

- The vaporization of silica rich-secondary phases at high sintering temperature involving the formation of porosities. Indeed, it is well admitted in literature [23] for low oxygen partial pressure ($PO_2 < 10^{-3}$ Pa) that weight loss becomes appreciable in Si-O system at temperature higher than 1800 K due to the formation of gaseous species such as SiO_(g).
- The final stage of the liquid-phase sintering of Nd:YAG specimens which would be preferentially reached at high soaking temperature could be accompanied by the coarsening of microstructure [24]. If the possibility of the Ostwald ripening presence is retained, it can be supposed that the residual pores would become larger leading to compact swelling.

The Arrhenius plot of the densification rate versus 1/T (see Fig. 6) provides a means for determining whether the process occurs by diffusion or interface-reaction controlled mechanism. Indeed, if densification is limited by diffusion of ionic species through the liquid phase, the activation energy of densification should be consistent with the activation energy for diffusion in liquid of such species. Besides, activation energies for the diffusion of Rare-Earth, Al³⁺ or O²⁻, in aluminosilicate glasses reported in literature did not exceed 350 kJ mol⁻¹ [25,26]. Therefore, if the dissolution rate of the solid-liquid interface represents the rate-limiting step of the Nd:YAG densification, the activation energy of densification should be in a good agreement with the activation energy for dissolution of YAG or the rare-earth element in glass. From Fig. 6, the measured activation energies are 1145 ± 90 and

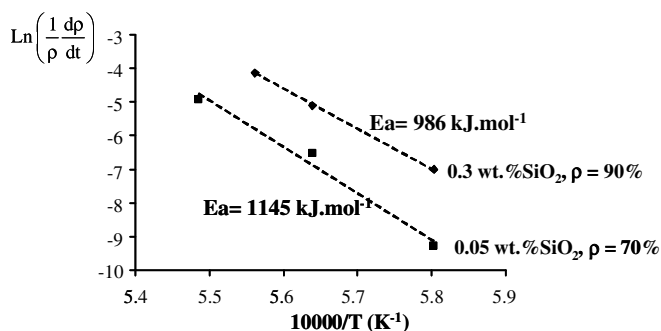


Fig. 6. Activation energy measurements for solution-precipitation stage during the liquid-phase sintering of silica-doped Nd:YAG ceramics.

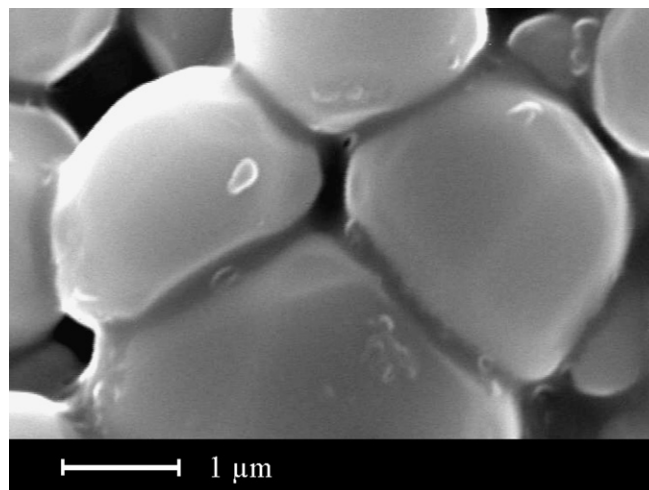


Fig. 7. SEM observation of Nd:YAG doped with 0.3 wt.% SiO₂, sintered under vacuum at 1800 K for 15 minutes, then etched 20 minutes at 1700 K under air.

986 ± 50 kJ mol⁻¹ for 0.05 wt.% and 0.3 wt.% SiO₂, respectively. So, the large activation energies measured during this study suggests that the diffusion process is not the limiting process. Furthermore, the activation energies for the dissolution of rare-earth element oxides [27] (*i.e.* » 1000 kJ mol⁻¹) are comparable with the present values of activation energies of densification.

The examination of the microstructural changes during the intermediate stage of liquid-phase sintering of Nd:YAG ceramics reported in Fig. 7 reveals that the particles contacts are flattened substantially, thus extensive solution-precipitation mechanism was operative. It is believed that Fig. 7 is the first microstructural evidence of contact point flattening by solution-precipitation process during the sintering of Nd:YAG specimens with silica.

4. Conclusion

The role of silica on the densification mechanism of Nd:YAG has been studied in isothermal conditions and under vacuum for temperatures ranging between 1773 and 1873 K. These temperatures were chosen because they lead to the formation of a liquid phase which results from the reaction between Nd:YAG and silica.

Instantaneous densification rates were analyzed with a conventional solid-state sintering model for undoped Nd:YAG ceramics. The mechanism controlling the densification during the intermediate stage of the solid-state sintering ($70\% \leq \rho \leq 90\%$) has been determined. The grain boundary diffusion of the rare-earth element (Y³⁺, Nd³⁺) would be responsible for the densification of undoped Nd:YAG specimens.

In the same way, isothermal experiments have been performed to elucidate the mechanism of Nd:YAG liquid-phase sintering. It is observed that the densification rate increases with increasing amount of silica as a result of both the decreased fractional solid-solid contact area and the enhancement of the kinetic of mass transport by diffusion through the liquid phase. The values of activation energies were determined to be around 1000 kJ mol⁻¹. It is concluded that the densification during the liquid-phase sintering of Nd:YAG ceramics is controlled by the interface reaction.

Acknowledgments

The authors make a point of thanking Dr. Bernard Soulestin, Dr. Daniel Tétard and Dr. Gérard Laborderie (SPCTS, UMR CNRS 6638, University of Limoges, France) for samples preparation and

their technical assistance during sintering treatments. The authors are also grateful to Dr. Jaafar Ghanbaja (Service Commun de Microscopie, CNRS UMR 7555, Nancy, France) for TEM analyses.

References

- [1] J. Lu, M. Prabhu, J. Song, Ch. Li, J. Xu, K.-I. Ueda, A. Kaminskii, H. Yagi, T. Yanagitani, *Appl. Phys. B* 71 (2000) 469.
- [2] S.-H. Lee, S. Kochawattana, G.L. Messing, J.Q. Dumm, G. Quarles, V. Castillo, *J. Am. Ceram. Soc.* 89 (2006) 1945.
- [3] A. Ikesue, Y.L. Aung, *J. Am. Ceram. Soc.* 89 (2006) 1936.
- [4] A. Ikesue, T. Kinoshita, K. Kamata, K. Yoshida, *J. Am. Ceram. Soc.* 78 (4) (1995) 1033.
- [5] J. Lu, K.-I. Ueda, H. Yagi, T. Yanagitani, Y. Akiyama, A.A. Kaminskii, *J. Alloy Compd.* 341 (2002) 220.
- [6] T. Feng, J. Shi, J. Chen, D. Jiang, *J. Mat. Res.* 20 (9) (2005) 2322.
- [7] C. Sallé, A. Maître, J.-F. Baumard, Y. Rabinovitch, *Opt. Rev.* 14 (4) (2007) 169.
- [8] K.M. Kinsman, J. McKittrick, E. Sluzky, K. Hesse, *J. Am. Ceram. Soc.* 77 (11) (1994) 2866.
- [9] G. De With, H.J.A. Dijk, *Mat. Res. Bull.* 19 (1984) 1669.
- [10] A. Ikesue, K. Yoshida, T. Yamamoto, I. Yamaga, *J. Am. Ceram. Soc.* 80 (6) (1997) 1517.
- [11] A. Maître, C. Sallé, R. Boulesteix, J.-F. Baumard, Y. Rabinovitch, *J. Am. Ceram. Soc.* 91 (2) (2008) 406.
- [12] A. Bondar, F.Ya. Galakhov, *Izv. Akad. Nauk SSSR, Ser. Khim* 7 (1964) 1325.
- [13] U. Kolitsch, H.J. Seifert, T. Ludwig, F. Aldinger, *J. Mater. Res.* 14 (2) (1999) 447.
- [14] G. De With, *Philips J. Res.* 42 (1987) 119.
- [15] A. Ikesue, K. Kamata, *J. Ceram. Soc. Jpn.* 103 (5) (1995) 489.
- [16] J.W. Vrolijk, S. Van Dem Cruisem, R. Metselaar, *Ceram. Trans.* 51 (1995) 573.
- [17] M.M. Kuklja, *J. Phys.: Condens. Matter* 12 (2000) 2953.
- [18] Y. Rabinovitch, D. Tétard, M.D. Faucher, M. Pham-Ti, *Opt. Mater.* 24 (1–2) (2003) 345.
- [19] H. Su, D.L. Johnson, *J. Am. Ceram. Soc.* 79 (1996) 3211.
- [20] P.-L. Chen, I.-W. Chen, *J. Am. Ceram. Soc.* 80 (1997) 637.
- [21] M. Jiménez-Melendo, H. Haneda, *J. Am. Ceram. Soc.* 84 (10) (2001) 2356.
- [22] R. Boulesteix, A. Maître, J.-F. Baumard, Y. Rabinovitch, S. Weber, M. Kilo, *Acta Mater.*, submitted for publication.
- [23] A.H. Heuer, V.L.K. Lou, *J. Am. Ceram. Soc.* 73 (10) (1990) 2785.
- [24] M.N. Rahaman, *Sintering of Ceramics*, CRC Press, New York, 2008, pp.180-182.
- [25] O.H. Kwon, G.L. Messing, *J. Am. Ceram. Soc.* 73 (2) (1990) 275.
- [26] K. Muehlenbachs, H.A. Schaeffer, *Can. Miner.* 15 (1977) 179.
- [27] Y. Zhang, A. Navrotsky, H. Li, L. Li, L.L. Davis, D.M. Strachan, *J. Non-Cryst. Solids* 296 (2001) 93.